Combining inhomogeneous magnetization transfer and multipoint Dixon acquisition: potential utility and evaluation

Ercan, E.; Varma, G.; Dimitrov, I.E.; Xi, Y.; Pinho, M.C.; Yu, F.F.; ... ; Vinogradov, E.

Combining inhomogeneous magnetization transfer and multipoint Dixon acquisition: Potential utility and evaluation

Ece Ercan[1,2] 🆔 🐦 | Gopal Varma[3] 🆔 | Ivan E. Dimitrov[4,5] 🆔 | Yin Xi[1,6] 🆔 | Marco C. Pinho[1,4] 🆔 | Fang F. Yu[1] 🆔 | Shu Zhang[1,7] 🆔 | Xinzeng Wang[1,8] 🆔 | Ananth J. Madhuranthakam[1,4] 🆔 | Robert E. Lenkinski[1,4] | David C. Alsop[3] 🆔 | Elena Vinogradov[1,4] 🆔

[1]Department of Radiology, UT Southwestern Medical Center, Dallas, TX, USA

[2]C.J. Gorter Center for High Field MRI, Department of Radiology, Leiden University Medical Center, Leiden, the Netherlands

[3]Division of MR Research, Beth Israel Deaconess Medical Center, Harvard Medical School, Radiology, Boston, MA, USA

[4]Advanced Imaging Research Center, UT Southwestern Medical Center, Dallas, TX, USA

[5]Philips Healthcare, Gainesville, FL, USA

[6]Department of Population and Data Sciences, UT Southwestern Medical Center, Dallas, TX, USA

[7]Department of Cancer Systems Imaging, UT MD Anderson Cancer Center, Houston, TX, USA

[8]Global MR Application and Workflow, GE Healthcare, Houston, TX, USA

Correspondence
Ece Ercan, C.J. Gorter Center for High
Field MRI, Department of Radiology, C3Q,
Leiden University Medical Center, P.O. Box
9600, 2300 RC, Leiden, the Netherlands.
Email: a.e.ercan@lumc.nl

Purpose: The recently introduced inhomogeneous magnetization transfer (ihMT) method has predominantly been applied for imaging the central nervous system. Future applications of ihMT, such as in peripheral nerves and muscles, will involve imaging in the vicinity of adipose tissues. This work aims to systematically investigate the partial volume effect of fat on the ihMT signal and to propose an efficient fat-separation method that does not interfere with ihMT measurements.

Methods: First, the influence of fat on ihMT signal was studied using simulations. Next, the ihMT sequence was combined with a multi-echo Dixon acquisition for fat separation. The sequence was tested in 9 healthy volunteers using a 3T human scanner. The ihMT ratio (ihMTR) values were calculated in regions of interest in the brain and the spinal cord using standard acquisition (no fat saturation), water-only, in-phase, and out-of-phase reconstructions. The values obtained were compared with a standard fat suppression method, spectral presaturation with inversion recovery.

Results: Simulations showed variations in the ihMTR values in the presence of fat, depending on the TEs used. The IhMTR values in the brain and spinal cord derived from the water-only ihMT multi-echo Dixon images were in good agreement with values from the unsuppressed sequence. The ihMT–spectral presaturation with inversion recovery combination resulted in 24%-35% lower ihMTR values compared with the standard non-fat-suppressed acquisition.

Conclusion: The presence of fat within a voxel affects the ihMTR calculations. The IhMT multi-echo Dixon method does not compromise the observable ihMT effect and can potentially be used to remove fat influence in ihMT.

KEYWORDS

fat suppression, ihMT, mDixon, myelin imaging

1 | INTRODUCTION

Inhomogeneous magnetization transfer (ihMT) provides novel contrast originating from the nonaveraged residual dipolar couplings within tissues.[1-3] In contrast to traditional magnetization transfer (MT) and quantitative MT methods, ihMT is attributable to dipolar order from residual dipolar interactions in tissue. The ihMT ratio (ihMTR) has been used as a convenient model-free measure of the effect. Human and animal studies of brain[1,2,4] and spinal cord[5-7] have demonstrated the sensitivity of ihMT to myelin content. Experimental studies[3] support membrane lipids, which are a major constituent of myelin, as the primary source of ihMT signal. Recent studies have shown that ihMT can be tuned to generate contrast in a range of tissues with different dipolar order (from white matter [WM] to muscles) using pulsed ihMT preparation and adjusting the interpulse delay to induce dipolar-order relaxation-time (ie, T_{1D}) weighting.[8,9] This opens new avenues for ihMT applications in the body, including quantitative imaging of peripheral nerves and human skeletal muscles.

The IhMT applications outside of the central nervous system would involve imaging in close proximity to adipose tissue (which is found near nerves and muscles) and may be further complicated by infiltration into the surrounding fat by different pathologies.[10] The presence of fat is known to create chemical shift artifacts and compromise tissue characterization.[11-13] Moreover, neuroradiological studies of the head and neck routinely use fat-suppression methods that improve visualization of pathology.[14-16] The ihMT effect is expected to be low in adipose tissues due to the relatively higher mobility of lipid molecules in fat droplets, compared with membrane lipids (eg, myelin). At the same time, the proximity to adipose tissue can result in partial volume effects, potentially deteriorating image quality and ihMTR values. However, the incorporation of fat suppression into the ihMT acquisition and its influence on ihMTR values have so far not been studied. These issues need to be addressed systematically to expand the applications of the ihMT technique.

The main aims of this study were (a) to investigate how the presence of fat in a voxel affects the observed ihMT signal using simulations, and (b) to evaluate the combination of ihMT, applied in previously documented central nervous system tissues, with two different fat-suppression strategies: the multi-echo Dixon (mDixon) technique[17] and the spectral presaturation with inversion recovery (SPIR) technique.

These methods were tested in anatomical regions with a well-established ihMT effect (ie, the human brain and spinal cord).

2 | METHODS

2.1 | Theory

The ihMT difference (ihMTD) is defined as

$$ihMTD = MT^+ + MT^- - MT^{+-} - MT^{-+}, \quad (1)$$

where MT^+, MT^-, MT^{+-}, and MT^{-+} correspond to the signals obtained using a single positive, single negative, simultaneous dual (alternating between positive and negative), and simultaneous dual (alternating between negative and positive) off-resonance RF frequency saturation, respectively.[18] Typically, the normalized ihMTR is used for quantification of the ihMT effect as follows:

$$ihMTR \equiv \frac{ihMTD}{S_0} = \frac{(MT^+ + MT^- - MT^{+-} - MT^{-+})}{S_0}, \quad (2)$$

where S_0 is a reference signal obtained with no saturation.

To investigate the influence of fat on the ihMT signal, we considered three pools: a free-water pool, a macromolecular bound pool with dipolar order, and a fat pool. For a voxel containing all three pools, the signal without saturation (S_0) can be expressed as

$$S_0 = S_w + S_f e^{-2\pi i \Delta f_{wf} TE}, \quad (3)$$

where Δf_{wf} is the frequency difference between water and fat, and S_w and S_f are the signal amplitudes from the water and fat pools, respectively. Assuming that (a) fat does not exchange magnetization with either the free-water or macromolecular bound pool,[11,19,20] and (b) the RF frequency of the ihMT preparation module is too far off-resonance to affect the fat pool directly, the signal with a single off-resonance frequency saturation can be expressed as

$$MT^+ = MT_w^+ + S_f e^{-2\pi i \Delta f_{wf} TE}, \quad (4)$$

where MT_w^+ corresponds to the signal obtained from the water pool after the single positive off-resonance RF frequency

saturation. Similar expressions can be used for MT^-, MT^{+-}, and MT^{-+}. Under these assumptions, the contribution of fat signal to the numerator of the ihMTR (Equation 2) cancels, while contribution to the denominator remains. However, magnitude images are often used for the ihMT calculation; therefore, the presence of adipose tissue will affect both the numerator and denominator of the ihMTR calculation as follows:

$$ihMTR = \frac{\left| MT_w^+ + S_f e^{-2\pi i \Delta f_{wf} TE} \right| + \left| MT_w^- + S_f e^{-2\pi i \Delta f_{wf} TE} \right| - \left| MT_w^{+-} + S_f e^{-2\pi i \Delta f_{wf} TE} \right| - \left| MT_w^{-+} + S_f e^{-2\pi i \Delta f_{wf} TE} \right|}{\left| S_w + S_f e^{-2\pi i \Delta f_{wf} TE} \right|}. \tag{5}$$

The modulus of the signals in this equation denotes the use of magnitude images in the ihMTR calculation.

2.2 | Simulation

In simulating the system, we considered three pools: free-water pool, macromolecular bound pool with dipolar order, and adipose fat pool. The water ihMT signal was modeled using the single-bound-pool Morrison model.[9,21] Because the fat pool is not coupled with the other two, its influence was added as a separate pool in the final calculation of the acquired signal (Equation 3). The ihMTD and ihMTR were calculated for the TEs used in in vivo experiments (TE = 1.5/2.5/3.5 ms), and for the optimal in-phase (TE = 2.3 ms) and out-of-phase (TE = 1.1 ms) conditions, as a function of increasing fat fraction, using Equation (5). Simulation parameters are reported in the Supporting Information.

2.3 | Magnetic resonance imaging scans

All experiments were performed on a 3T Ingenia Philips MRI scanner (Philips Healthcare, Best, Netherlands) using a 32-channel receive head coil and multitransmit body coil. The ihMT-mDixon sequence was applied on 9 healthy volunteers (4 male, 5 female; age: 26 ± 2 years). Six of the volunteers underwent a brain scan, and the remaining 3 volunteers underwent a cervical spinal cord scan. The study adhered to the local institutional review board guidelines, and written informed consent was obtained from all volunteers.

2.4 | The ihMT-mDixon sequence

A steady-state 3D ihMT spoiled gradient-echo sequence[18,22] was combined with a multi-echo Dixon acquisition. The ihMT preparation parameters are reported in the Supporting

Information. A reference image (S_0) and four separate images for ihMT (frequency offsets: +7 kHz [MT^+], −7 kHz [MT^-], alternating ±7 kHz [MT^{+-}], and alternating ∓7 kHz [MT^{-+}] respectively), were obtained at each TE of the multi-echo acquisition. The acquisition parameters used in the experiments are listed in Supporting Information Table S1.

2.5 | Comparison of ihMT-mDixon with ihMT and SPIR combined sequences

To compare the effects of the mDixon technique with that of spectral fat suppression, data were acquired in the brains of 2 healthy volunteers while adding (a) a SPIR module before the ihMT preparation (SPIR-ihMT) and (b) a SPIR module after the ihMT preparation and before the acquisition of one line of k-space (ihMT-SPIR), in addition to mDixon-ihMT. All other acquisition parameters were kept the same for all three suppression schemes (Supporting Information Table S1).

2.6 | Postprocessing and data analysis

From the ihMT-mDixon acquisition, the in-phase (IP), out-of-phase (OP), fat-only (F), and water-only (W) images were reconstructed by the standard manufacturer processing using the seven-peak fat model.[23] Equation (2) was used to calculate the ihMTR values for each voxel (a) from the original (non-Dixon) reconstructions without fat suppression (echo 1 [E1], echo 2 [E2], and echo 3 [E3], respectively), (b) from IP, OP, F, and W reconstructions, and (c) from the SPIR-ihMT and ihMT-SPIR acquisitions.

Regions of interest (ROIs) were manually drawn in WM regions for each volunteer. The mean ihMTR values were calculated from ROIs separately for IP, OP, and W reconstructions, as well as the original acquisitions (E1, E2, and E3). Bland-Altman analysis was performed using all voxels from the same subject to assess the bias between W and E1 reconstructions for each subject.

A mixed-effects model was used to estimate the voxel-wise mean difference and 95% confidence intervals (CIs) between different acquisitions and reconstruction methods. For brain WM, different subjects and ROIs within subjects served as random effects. For the comparison of different fat-suppression methods from the same volunteer, ROIs were used as random effects. All analyses were performed using *SAS 9.4* (SAS Institute, Cary, NC).

3 | RESULTS

3.1 | Simulation

Figure 1 demonstrates the dependence of ihMTD and ihMTR values on fat fraction from simulations. Supporting Information Figure S1 shows changes in S_0 as a function of fat fraction. More detailed analysis is provided in the Supporting Information. The ihMTD values observed in the IP condition (IP-ihMTD) decrease steadily (dark blue lines in Figure 1A), reflecting the decrease in water fraction. Similar behavior was observed for E2 (TE = 2.5 ms; green line in Figure 1A), which has a TE close to that of the IP condition (2.3 ms). The same behavior was observed for IP-ihMTR, following normalization by S_0 (total signal without saturation). Normalization by the water-only signal (Figure 1B) leads to a different curve behavior, as both the numerator and denominator decreased linearly. It is important to note that if the myelinated tissue remains unchanged, ihMTD and ihMTR should not change with changing fat fraction. Thus, just acquiring data at IP condition will not produce correct ihMT values.

The behavior under OP conditions (OP-ihMTD and OP-ihMTR) was more complicated (orange lines in Figure 1). The OP-ihMTD values were observed to decrease and undergo a discontinuous sign change, which is associated with the use of absolute values. The exact crossing point depends on the bound pool fraction and strengths of bound pool interactions (as demonstrated by changes in T_{1D}). When the simulated T_{1D} values were increased, the zero-crossing also increased (see Supporting Information Figures S2 and S3). In addition, a singularity point is expected for OP-ihMTR images at a fat fraction of 50%, due to normalization by a zero S_0 value (Figure 1B, Supporting Information Figure S1).

More details and analytical expressions can be found in the Supporting Information.

3.2 | Human studies

Figure 2 demonstrates a comparison of ihMTR maps obtained from the brain of a healthy volunteer using E1 (TE = 1.5 ms) and the W reconstruction. A very small difference (<1% ihMTR) was observed when the latter was subtracted from the ihMTR map obtained from E1. Mean ihMTR values calculated from ROIs in the WM were very similar among IP, OP, W, and E1 conditions across all volunteers (Figures 3 and 5), averaging 7.4% ± 0.4%. This is expected due to the lack of fat in brain tissue (Supporting Information Figure S4). Figure 4, Supporting Information Figure S5, and Figure 5 show a typical ihMTR map and WM ihMTR values obtained from the spinal cord of the volunteers. A small bias (in the range of SD) was observed between ihMTRs obtained from W and E1 reconstructions (Supporting Information Table S2, Figures S6 and S7). Of note, it can be seen that the application of the mDixon method effectively suppresses subcutaneous fat within the face and upper neck on the W reconstruction.

3.3 | Comparison of ihMT-mDixon with ihMT and SPIR combined sequences

Supporting Information Figure S8 shows ihMTR maps from a single brain slice of one of the volunteers, as well as box plots from three ROIs obtained with and without fat-suppression methods. The ihMTR map obtained without fat suppression (E1) shows comparable contrast to the W-ihMTR map calculated from ihMT-mDixon. However, combining ihMT with
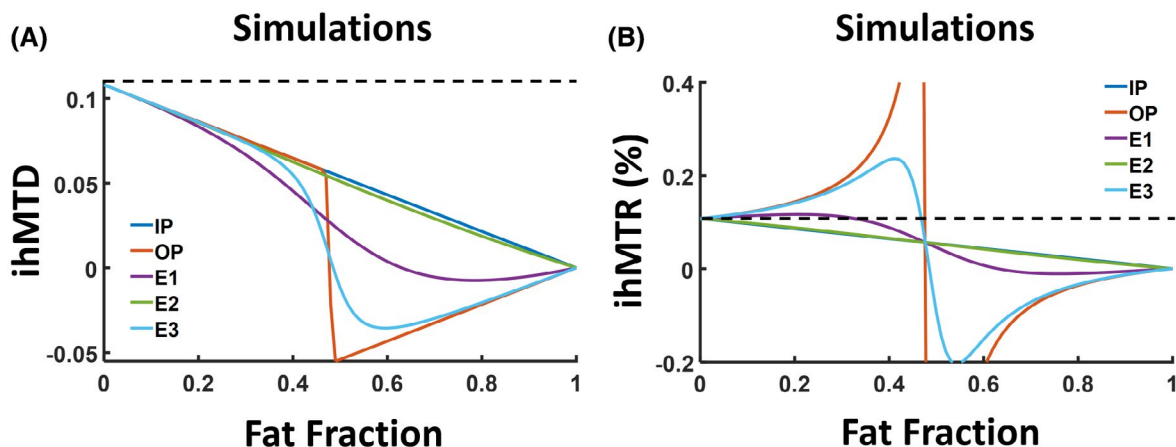
FIGURE 1 Simulations of inhomogeneous magnetization transfer difference (ihMTD) (A) and inhomogeneous magnetization transfer ratio (ihMTR) (B) as a function of the fat fraction for different TE values: 2.2 ms (in-phase [IP], dark blue), 1.1 ms (out-of-phase [OP], orange), 1.5 ms (echo 1 [E1], purple), 2.5 ms (echo 2 [E2], green), and 3.5 ms (echo 3 [E3], light blue). The simulated ihMTR values of IP (dark blue) and E2 (green) overlapped. The dashed lines in (A) and (B) show ihMTD value for fat fraction = 0 (upper limit)

FIGURE 2 A,B, The ihMTR maps from original (non-Dixon) E1 and water-only (W) reconstructions obtained from the brain of a healthy volunteer. C, Difference between these two maps

FIGURE 3 A, Representative regions of interest (ROIs) (left [ROI1] and left [ROI2]) internal capsules, genu [ROI3] and splenium [ROI4] of the corpus callosum) in white matter (WM) are illustrated in the ihMTR map of the brain from one of the volunteers. B-E, Box plots showing normalized ihMTR values for E1, E2, and E3 acquisitions and IP and OP reconstructions normalized to W reconstructions
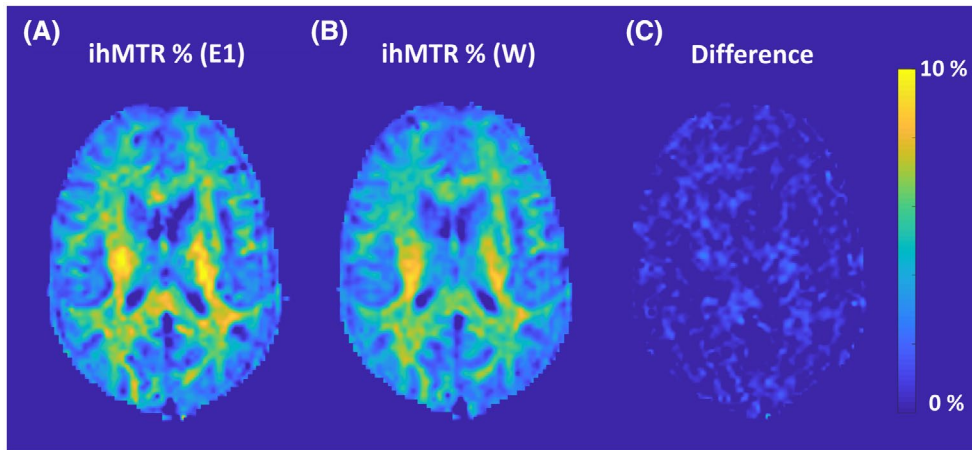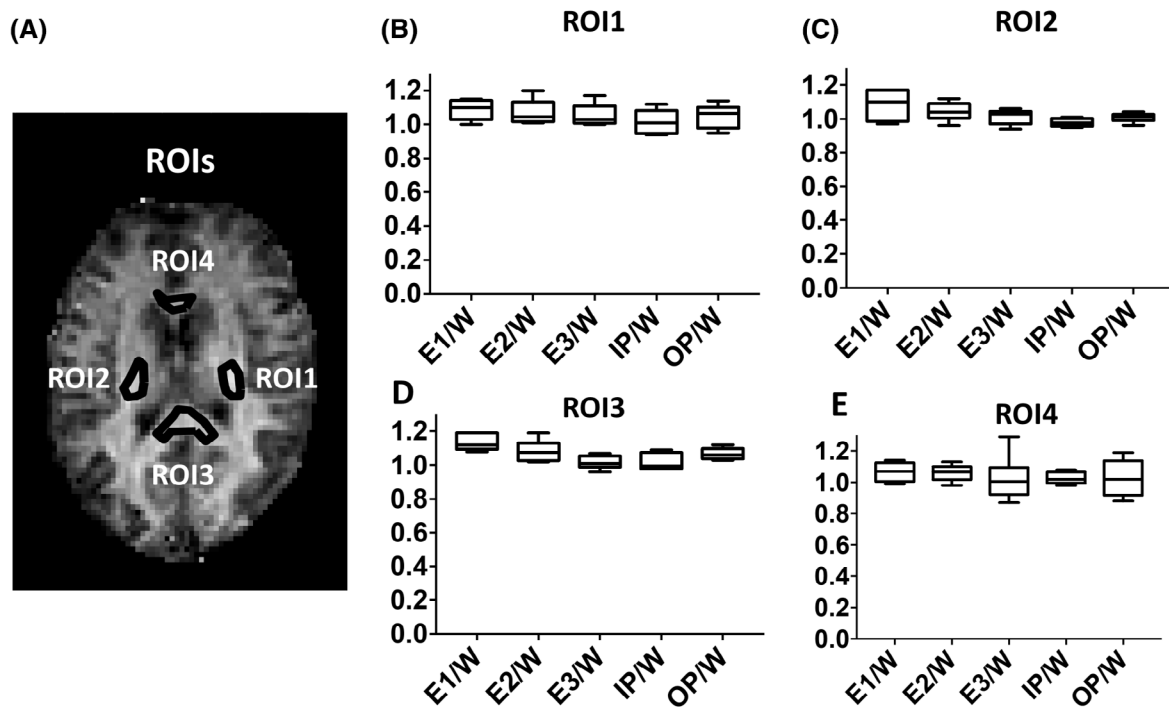
SPIR suppression resulted in ihMTR maps with consistently lower ihMTR values and larger SDs, regardless of whether the SPIR pulse followed or proceeded off-resonance RF irradiation (ie, ihMT-SPIR or SPIR-ihMT). Statistical analysis on pairwise difference showed that, on average, in ihMTR absolute scale, ihMTR values obtained from E1 were 2.9% higher than those from SPIR_ihMT (CI: 2.7%, 3.1%) and 2.0% higher than those from ihMT_SPIR (CI: 1.8%, 2.2%), compared with only 0.5% higher than those from W-ihMTR (CI: 0.3, 0.7). This corresponds to a 24%-35% fractional

change relative to E1 and correspondingly lower ihMTR values when using SPIR compared to the case without fat suppression (E1). In contrast, ihMT-mDixon resulted in only 6% fractional change relative to E1.

4 | DISCUSSION

In this study, we investigated the influence of fat on the observed ihMTR values and evaluated multi-echo Dixon and
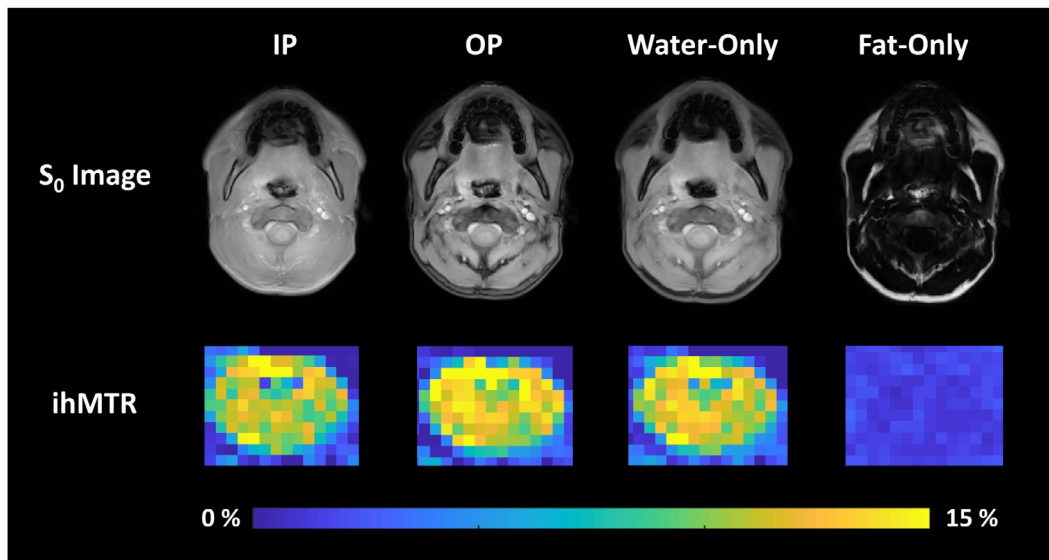
IP
OP
Water-Only
Fat-Only
S0 Image
ihMTR
0 %
15 %

FIGURE 4 Reference (S_0) images (top row) and ihMTR (middle and bottom row) maps obtained from IP, OP, W, and fat-only (F) reconstructions obtained from one slice through the C2-C3 region of the cervical spinal cord of a healthy volunteer. The ihMTR maps were zoomed-in to show the values within the spinal cord

Brain
E1
IP
OP
W
ihMTR (%)
15
10
5
0
1
2
3
4
5
6
Subject #
Spinal Cord
E1
IP
OP
W
ihMTR (%)
15
10
5
0
7
8
9
Subject #

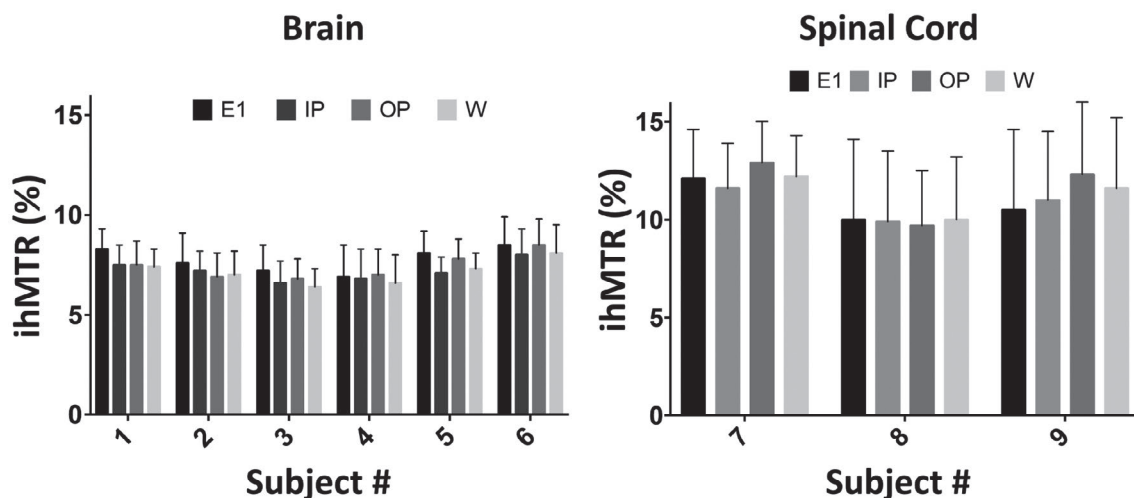

FIGURE 5 Mean ihMTR values (in percentage) and their SDs within manually drawn ROIs from the brain (A) and spinal cord (B) WM from each healthy volunteer. The reported values reflect the mean ihMTR values obtained from all voxels within all four ROIs and their SDs per subject. The ihMTR values are displayed separately for the original acquisition at E1 and the multi-echo Dixon (mDixon) IP, OP, and W reconstructions

SPIR fat-suppression methods in combination with the recently introduced steady-state 3D ihMT sequence.[18,22] In the presence of fat, ihMTD and ihMTR become strongly dependent on the acquisition TE.

This study emphasizes the importance of using water-only images for proper normalization of the ihMTR values. The contribution of fat to the ihMT signal has not previously been investigated. Previous studies of MT,[11,24] CEST,[25] and quantitative MT[26] imaging showed evidence of variation on MTR, $\mathrm{MTR}_{\mathrm{asym}}$, and quantitative MT values, depending on the fat fraction in the corresponding voxel. While similar to ihMT, these sequences rely on different chemical or physical principles and use different postprocessing, thus demonstrating salient differences with respect to the influence of fat. Similar to the observations in the CEST study, we observed a linear decrease in the ihMTR for the in-phase condition. The linear decrease is attributed to the monotonic decrease of the water pool size in the IP condition,[25] only if normalized by the total signal. However, normalization by total signal, including fat, will lead to an erroneous result, even if complex postprocessing is used, which may cancel out some of the fat contribution.

The OP condition demonstrated more complex behavior, with a singularity at equal fat and water fractions, due to

normalization with zero values. The distinguishing aspect in our study is focused on ihMTD (Equation 1) and the observation that fat influences its behavior, and not only the normalization factor (denominator, Equation 2). This is because in our study (as well as in most common ihMT postprocessing), magnitude images were used. Thus, the influence of fat may lead to erroneous ihMTD and ihMTR values (Equation 5). The use of complex images could eliminate the fat contribution, but normalization by pure water signal would be required to get exact ihMTR values. The proper normalization will become exceedingly important with the further development of quantification methods. Thus, mDixon can provide a convenient way of eliminating the influence of fat and obtaining accurate ihMTR values near adipose tissues.

The ihMTR values obtained from the WM brain regions were consistent with those obtained from similar regions in a previous study.[18] Bland-Altman results showed a small bias (within the range of SD) between ihMTR values obtained with mDixon and original acquisitions, with W-ihMTR slightly lower than E1-ihMTR. This bias could be attributed to an error propagation during the model fitting used for mDixon, as well as during the ihMTR calculation. Another possible explanation for the small bias is the transverse relaxation of myelin water. Although the water compartment, which gives rise to the ihMT signal, has not yet been fully investigated, MT between the macromolecular pool and myelin water pool has already been shown[27] and is expected to contribute to the resulting ihMT effect. The T_2^* relaxation of myelin water during the multi-echo acquisition might, therefore, add a small bias to the calculated ihMTR. Inclusion of T_2^* decay of both myelin water and intra/extracellular water in the Dixon model may help correct for this small bias.

Our results further demonstrate that mDixon performs better than SPIR when combined with the ihMT sequence. Combining ihMT with SPIR resulted in lower ihMT ratios, which may be indicative of direct water saturation or saturation of broad macromolecular lines while using SPIR.

It is important to note that this represents one of the first reported applications of a 3D steady-state ihMT acquisition in the spinal cord,[28,29] with previous ihMT studies using a prolonged saturation train followed by the 2D spin-echo acquisition of a single slice.[5-7] The spinal cord ihMTR values obtained in this study were 40%-60% higher than those reported in previous studies using prolonged saturation.[5-7] The higher ihMT values obtained in our study are in line with increases in ihMT signal by manipulation of the duty cycle,[22,30,31] although our sequence had some slight differences in pulse width, interpulse TR, number of pulses, and B_{1rms} compared with the sequence used in these studies. Higher SDs for ihMT observed in the spinal cord compared with the brain WM indicate that the sequence should be further optimized for a more robust application in the spinal cord. Additional strategies such as using a spinal cord coil,

more averaging, and synchronization with pulsation could help to reduce the SD in future studies.[5]

We chose to image the brain and spinal cord to demonstrate the feasibility of the ihMT-mDixon method. The in vivo applications in this study did not focus on muscles or nerves, because we wished to demonstrate that the ihMT-mDixon technique did not adversely affect the ihMT signal calculated relative to ihMT combined with fat suppression by SPIR. We acknowledge that application of ihMT in peripheral structures outside of the central nervous system have additional challenges due to physiological motion, low SNR, B_0 and B_1 inhomogeneities, and complexities involved with tailoring the sequence for targeted T_{1D} values (eg, the relatively short T_{1D} of muscles[8,31]). Additionally, the simulations in this study assumed a simple fat-water model with a single fat peak at −3.4 ppm from the water peak. Advanced Dixon reconstruction models include multiple fat peaks[23] and could be tailored for a specific fat composition. Such models may improve the accuracy of the results. Future studies are necessary to optimize ihMT for applications in muscles and nerves, and therefore further develop the proposed ihMT-mDixon method. Future directions will involve using ihMT-mDixon for truncated FOV applications in spinal cord, and further optimization and combination with motion correction methods to demonstrate ihMT-mDixon in structures adjacent to fat (eg, nerves).

5 | CONCLUSIONS

The presence of fat within a voxel affects the ihMTR calculations and leads to a dependence on the TE. Combining the 3D steady-state ihMT sequence with the multi-echo Dixon acquisition (ihMT-mDixon) provides effective fat suppression without increasing the scan time or specific absorption rate, and without compromising the observable ihMT effect. We expect this method to be beneficial in future applications of ihMT for imaging peripheral nerves and muscles, which are situated within the proximity of high adipose tissue content.

ORCID

Ece Ercan https://orcid.org/0000-0002-8187-2075
Gopal Varma https://orcid.org/0000-0002-7060-1982
Ivan E. Dimitrov https://orcid.org/0000-0003-2686-6884

Yin Xi ![ORCID] https://orcid.org/0000-0001-9743-3010
Marco C. Pinho ![ORCID] https://orcid.org/0000-0002-4645-1638
Fang F. Yu ![ORCID] https://orcid.org/0000-0001-9913-1331
Shu Zhang ![ORCID] https://orcid.org/0000-0003-0433-1977
Xinzeng Wang ![ORCID] https://orcid.org/0000-0002-0415-7246
Ananth J. Madhuranthakam ![ORCID] https://orcid.
org/0000-0002-5524-7962
David C. Alsop ![ORCID] https://orcid.org/0000-0002-8206-1995
Elena Vinogradov ![ORCID] https://orcid.
org/0000-0003-4607-4147

TWITTER

Ece Ercan ![Twitter] @aeceercan

REFERENCES

1. Varma G, Duhamel G, de Bazelaire C, Alsop DC. Magnetization transfer from inhomogeneously broadened lines: a potential marker for myelin. *Magn Reson Med*. 2015;73:614-622.
2. Girard OM, Prevost VH, Varma G, Cozzone PJ, Alsop DC, Duhamel G. Magnetization transfer from inhomogeneously broadened lines (ihMT): experimental optimization of saturation parameters for human brain imaging at 1.5 Tesla. *Magn Reson Med*. 2015;73:2111-2121.
3. Swanson SD, Malyarenko DI, Fabiilli ML, Welsh RC, Nielsen J-F, Srinivasan A. Molecular, dynamic, and structural origin of inhomogeneous magnetization transfer in lipid membranes. *Magn Reson Med*. 2017;77:1318-1328.
4. Prevost VH, Girard OM, Varma G, Alsop DC, Duhamel G. Minimizing the effects of magnetization transfer asymmetry on inhomogeneous magnetization transfer (ihMT) at ultra-high magnetic field (11.75 T). *Magn Reson Mater Phys Biol Med*. 2016;29:699-709.
5. Girard OM, Callot V, Prevost VH, et al. Magnetization transfer from inhomogeneously broadened lines (ihMT): improved imaging strategy for spinal cord applications. *Magn Reson Med*. 2017;77:581-591.
6. Taso M, Girard OM, Duhamel G, et al. Tract-specific and age-related variations of the spinal cord microstructure: a multi-parametric MRI study using diffusion tensor imaging (DTI) and inhomogeneous magnetization transfer (ihMT). *NMR Biomed*. 2016;29:817-832.
7. Rasoanandrianina H, Grapperon A-M, Taso M, et al. Region-specific impairment of the cervical spinal cord (SC) in amyotrophic lateral sclerosis: a preliminary study using SC templates and quantitative MRI (diffusion tensor imaging/inhomogeneous magnetization transfer). *NMR Biomed*. 2017;30:e3801.
8. Prevost VH, Girard OM, Mchinda S, Varma G, Alsop DC, Duhamel G. Optimization of inhomogeneous magnetization transfer (ihMT) MRI contrast for preclinical studies using dipolar relaxation time (T1D) filtering. *NMR Biomed*. 2017;30:e3706.
9. Varma G, Girard OM, Prevost VH, Grant AK, Duhamel G, Alsop DC. In vivo measurement of a new source of contrast, the dipolar relaxation time, T1D, using a modified inhomogeneous magnetization transfer (ihMT) sequence. *Magn Reson Med*. 2017;78:1362-1372.
10. Li KE, Dortch RD, Kroop SF, et al. A rapid approach for quantitative magnetization transfer imaging in thigh muscles using the pulsed saturation method. *Magn Reson Imaging*. 2015;33:709-717.
11. Li W, Wang X, Miller FH, Larson AC. Chemical shift magnetization transfer magnetic resonance imaging. *Magn Reson Med*. 2017;78:656-663.
12. Haase A, Frahm J, Hanicke W, Matthaei D. ^{1}H NMR chemical shift selective (CHESS) imaging. *Phys Med Biol*. 1985;30:341-344.
13. Frahm J, Haase A, Hänicke W, Matthaei D, Bomsdorf H, Helzel T. Chemical shift selective MR imaging using a whole-body magnet. *Radiology*. 1985;156:441-444.
14. Tien RD. Fat-suppression MR imaging in neuroradiology: techniques and clinical application. *Am J Roentgenol*. 1992;158:369-379.
15. Gaddikeri S, Mossa-Basha M, Andre JB, Hippe DS, Anzai Y. Optimal fat suppression in head and neck MRI: comparison of multipoint Dixon with 2 different fat-suppression techniques, spectral presaturation and inversion recovery, and STIR. *Am J Neuroradiol*. 2018;39:362-368.
16. Barger AV, DeLone DR, Bernstein MA, Welker KM. Fat signal suppression in head and neck imaging using fast spin-echo-IDEAL technique. *Am J Neuroradiol*. 2006;27:1292-1294.
17. Dixon WT. Simple proton spectroscopic imaging. *Radiology*. 1984;153:189-194.
18. Ercan E, Varma G, Mädler B, et al. Microstructural correlates of 3D steady-state inhomogeneous magnetization transfer (ihMT) in the human brain white matter assessed by myelin water imaging and diffusion tensor imaging. *Magn Reson Med*. 2018;80:2402-2414.
19. Chen J-H, Le HC, Koutcher JA, Singer S. Fat-free MRI based on magnetization exchange. *Magn Reson Med*. 2010;63:713-718.
20. Chen J-H, Sambol EB, DeCarolis P, et al. High-resolution MAS NMR spectroscopy detection of the spin magnetization exchange by cross-relaxation and chemical exchange in intact cell lines and human tissue specimens. *Magn Reson Med*. 2006;55:1246-1256.
21. Varma G, Girard OM, Prevost VH, Grant AK, Duhamel G, Alsop DC. Interpretation of magnetization transfer from inhomogeneously broadened lines (ihMT) in tissues as a dipolar order effect within motion restricted molecules. *J Magn Reson*. 2015;260:67-76.
22. Mchinda S, Varma G, Prevost VH, et al. Whole brain inhomogeneous magnetization transfer (ihMT) imaging: sensitivity enhancement within a steady-state gradient echo sequence. *Magn Reson Med*. 2018;79:2607-2619.
23. Eggers H, Brendel B, Duijndam A, Herigault G. Dual-echo Dixon imaging with flexible choice of echo times. *Magn Reson Med*. 2011;65:96-107.
24. Holmes JH, Johnson KM, Hernando D, Reeder SC, Samsonov A. *Magnetization transfer ratio (MTR) imaging in the presence of fat*. In: Proceedings of the Joint Annual Meeting of ISMRM-ESMRMB, Milan, Italy, 2014. p 3365.
25. Zhang S, Seiler S, Wang X, et al. CEST-Dixon for human breast lesion characterization at 3 T: a preliminary study. *Magn Reson Med*. 2018;80:895-903.
26. Smith AK, Dortch RD, Dethrage LM, et al. Incorporating Dixon multi-echo fat water separation for novel quantitative magnetization transfer of the human optic nerve in vivo. *Magn Reson Med*. 2017;77:707-716.
27. Vavasour IM, Whittall KP, Li DKB, MacKay AL. Different magnetization transfer effects exhibited by the short and long T2 components in human brain. *Magn Reson Med*. 2000;44:860-866.
28. Ercan E, Pinho MC, Varma G, et al. *3D steady-state inhomogeneous magnetization transfer (ihMT) gradient echo sequence for*

spinal cord imaging at 3T. In: Proceedings of the Joint Annual Meeting of ISMRM-ESMRMB, Paris, France, 2018. p 5502.

29. Varma G, Munsch F, Burns B, et al. Three-dimensional inhomogeneous magnetization transfer with rapid gradient-echo (3D ihM-TRAGE) imaging. *Magn Reson Med*. 2020;84:2964-2980.

30. Carvalho VND, Hertanu A, Grélard A, et al. MRI assessment of multiple dipolar relaxation time (T1D) components in biological tissues interpreted with a generalized inhomogeneous magnetization transfer (ihMT) model. *J Magn Reson*. 2020;311:106668.

31. Varma G, Girard OM, Mchinda S, et al. Low duty-cycle pulsed irradiation reduces magnetization transfer and increases the inhomogeneous magnetization transfer effect. *J Magn Reson*. 2018;296:60-71.

SUPPORTING INFORMATION

Additional supporting information may be found online in the Supporting Information section.

TABLE S1 Acquisition parameters for in vivo scans. Scan time includes acquisition of all five data sets (MT^+, MT^-, MT^{+-}, MT^{-+}, and S_0 image without the saturation, for calculation of inhomogeneous magnetization transfer rate [ihMTR])

TABLE S2 Mean difference (bias) and 95% confidence intervals obtained from the Bland-Altman plots obtained from the comparison of multi-echo Dixon water-only and original acquisitions. E1, echo 1; mDixon, multi-echo Dixon; W, water only

FIGURE S1 Simulations of signal without saturation (S_0) as a function of the fat fraction for different TE values: 2.2 ms (IP, dark blue), 1.1 ms (OP, orange), 1.5 ms (E1, purple), 2.5 ms (E2, green), and 3.5 ms (E3, light blue). Abbreviations: E1, echo 1; E2, echo 2; E3, echo 3; IP, in-phase; OP, out-of-phase

FIGURE S2 Simulations of inhomogeneous magnetization transfer difference (ihMTD; top) and inhomogeneous magnetization transfer ratio (ihMTR; bottom) as a function of the fat fraction for different TE values: 2.2 ms (IP, dark blue), 1.1 ms (OP, orange), 1.5 ms (E1, yellow), 2.5 ms (E2, purple), and 3.5 ms (E3, green) for different T_{1D} values. The simulated ihMTR values of IP (dark blue) and E2 (purple) overlap. The water-pool fraction (M_{0A}) and bound-pool fraction (M_{0B}) are 1.00 and 0.01, respectively. The dashed lines show the ihMTD value for fat fraction = 0 (upper limit)

FIGURE S3 Simulations of ihMTD (top) and ihMTR (bottom) as a function of the fat fraction for different TE values: 2.2 ms (IP, dark blue), 1.1 ms (OP, orange), 1.5 ms (E1, yellow), 2.5 ms (E2, purple), and 3.5 ms (E3, green) for different T_{1D} values. The simulated ihMTR values of IP (dark blue) and E2 (purple) overlapped. The water-pool fraction (M_{0A}) and bound-pool fraction (M_{0B}) are 1.000 and 0.139, respectively. The dashed lines show the ihMTD value for fat fraction = 0 (upper limit)

FIGURE S4 Fat fraction map of one slice from the brain of a healthy volunteer. Brain tissue displays 0% fat fraction

FIGURE S5 Reference (S_0) images (top row) and ihMTR (middle and bottom row) maps obtained from IP, OP, water-only (W), and fat-only (F) reconstructions obtained from one slice through the C2-C3 region of the cervical spinal cord of a healthy volunteer

FIGURE S6 Bland-Altman plots comparing brain white-matter ihMTR from mDixon W and E1 acquisitions in 6 healthy volunteers

FIGURE S7 Bland-Altman plots comparing spinal cord white-matter ihMTR from mDixon W and E1 acquisitions in 3 healthy volunteers

FIGURE S8 A, The ihMTR maps obtained from one slice of the brain of a healthy volunteer using three-point mDixon and spectral presaturation with inversion recovery (SPIR) fat-suppression methods. The inhomogeneous magnetization transfer (ihMT)-SPIR acquisition used spectral fat suppression after the ihMT preparation module, whereas SPIR-ihMT involved spectral fat suppression before the ihMT preparation. B, Box plots from three regions of interest obtained with and without fat-suppression methods. The values shown were obtained using Dixon IP, OP, and W reconstructions and acquisitions at different TEs (E1, E2, E3). Consistent undervaluing is seen with the use of spectral fat suppression